Research Article | Vol. 32, No. 15 / 15 Jul 2024 / Optics Express 26632
Optics EXPRESS

Photoluminescence probing of light absorption centers at silica laser damage

YOONSOO RHO,[1,2] MATTHIAS A. DAEUMER,[1] CHRISTOPHER F. MILLER,[1] CHRISTOPHER M. MAH,[1] TED A. LAURENCE,[1] CHRISTOPHER W. CARR,[1] AND JAE HYUCK YOO[1,*]

[1]*Physical & Life Sciences and NIF & Photon Sciences, Lawrence Livermore National Laboratory, Livermore, California 94550, USA*
[2]*Department of Mechanical Engineering, Ulsan National Institute of Science and Technology (UNIST), Ulsan, 44919, Republic of Korea*
[*]*yoo5@llnl.gov*

Abstract: We use photoluminescence (PL) imaging to study damage growth precursors within laser damage sites on the surface of silica. Damage site evolution is induced by multiple shots of UV nanosecond pulsed laser at various energy densities and monitored throughout the early stages of growth. Wide-field PL imaging rapidly locates microscopic light absorption centers within the silica damage site. Our quantitative analysis shows that damage sites with strong local PL intensity show a higher probability of growth upon subsequent laser pulses. Scanning electron microscopy (SEM) paired with a study of PL spectrum shows that the strong PL intensity appears from the subsurface fractures with high defect density, which provides a local light absorption center leading to significant damage growth. We believe that this result offers an efficient optical damage mitigation strategy by providing a rapid and non-destructive optical inspection approach.

1. Introduction

Mitigation of laser induced damage growth on the surface of dielectric optical components is critical toward the continued development of high-energy and high-power laser systems. Consequently, a variety of damage site mitigation strategies have been developed to prevent further growth such as surface polishing [1,2], chemical etching [3–6], thermal annealing [7], and CO_2 laser ablation (referred to as rapid ablation mitigation (RAM)) [8,9]. Damage sites with a larger effective circular diameter (ECD) have been shown to have a higher propensity to exhibit laser damage growth [10,11]. This could be due to the larger internal subsurface fractures containing a greater quantity of defects. Often, damage sites exposed to multiple laser shots show a sudden increase in their ECD after a single shot following negligible ECD change under prior shots [10,11]. Such stochastic growth behavior indicates that understanding local defect characteristics is important for growth prediction.

Photoluminescence imaging has been implemented to study the local chemical and structural precursors for laser damage growth in SiO_2. Initial work observed elevated PL intensities in laser-induced cracks and defects [12–14]. Local PL intensity variations are directly correlated to local plasma formation from the silica damage site during a nanosecond laser shot [12], indicating PL signatures can serve as an optical fingerprint of damage growth precursors. Furthermore, it has been shown that lifetime decay characteristics [15–17] and photochemical quenching behavior of PL [18] are associated with light absorption centers and local chemical and morphological properties related to laser damage growth. Although previous studies have provided insights into the correlation between PL and local defects and structures associated with laser damage growth, a quantitative study on how PL is connected to laser damage growth in a multi-shot process is still needed.

#527241 https://doi.org/10.1364/OE.527241
Journal © 2024 Received 18 Apr 2024; revised 24 May 2024; accepted 29 May 2024; published 9 Jul 2024

Optics EXPRESS

Here, we probe multi laser shot induced damage precursors at the surface of silica through wide-field PL intensity imaging. Throughout the laser shot sequence, local PL intensity changes without noticeable external growth of the damage site is observed. However, ECD growth that does eventually occur after multiple pulses can be anticipated through the analysis of the elevated local PL intensity before the shot that induces growth. Our quantitative analysis shows a strong correlation between the local PL intensity and probability to damage growth. Based on SEM analysis paired with a study of PL spectrum, we find that an elevated local PL intensity is due to subsurface fractures and cracks with a high defect density, facilitating significant damage growth upon a subsequent laser shot. The result provides a pathway to mitigating damage growth by non-destructive optical probing of damage precursors during multi-shot process in a high-energy and high-power laser system.

2. Experiment

Initial damage sites on silica surface (Corning 7980 with 2 inches of diameter and 1 cm of thickness) were generated by a single nanosecond pulse of UV laser irradiation [19,20]. Specifically, an Nd:glass amplifier laser system (λ ~355 nm (3.5 eV), 5 ns) with 1-cm diameter at an energy density of 25 J/cm^2 was used generating a large number of damage sites (typically 200–1000 damage sites) with an ECD of a few tens of μm on the exit surface. Then, damage growth and PL measurements are performed on a custom-built optical setup on the input surface of the laser damage site, as shown schematically in the Supplement 1 (Fig. S1).

The laser shot sequence for laser damage growth is performed through a combination of fixed and ramp-up fluence conditions using a UV nanosecond laser (CFR, Quantel, λ ~355 nm (3.5 eV), 7 ns) that is focused to a spot size of ~300 μm using a spherical lens. Initially, 4-5 shots of fixed fluence are illuminated at an individual damage site. The fluence ranged from 12-18 J/cm^2 depending on the experiment. In this range, the probability of growth is relatively low for an initial damage site with an ECD of 10~30 μm. Until significant growth is observed, subsequent series of shots with greater fluence are taken. Typically, the fluence was increased by 1 J/cm^2 for each subsequent 4-5 shot series.

Wide-field PL imaging of each damage site is performed before and after each nanosecond laser shot for damage growth with a cooled CMOS camera (Sona, Andor). The wide-field approach allows rapid imaging, typically less than 1 sec for a single damage site. The CW excitation laser (λ ~532 nm (2.35 eV) (Sprout-G, Light House), 1 W) is modified to be circular and spatially uniform with a homogenizer (RD-227-Q-Y-A, Holo/Or) and focused to a spot 30 μm in diameter with an infinity corrected objective lens (M Plan Apo 50X, Mitutoyo). A dichroic mirror (DMLP550, Thorlabs) reflects the laser beam to the sample, and transmits the generated PL signal on its return path to the CMOS camera after passing through a long pass filter (FELH0550, Thorlabs) and two notch filters (NF533-17, Thorlabs) that block the excitation laser beam. Optical reflectance images are also taken at each location, which helps accurately register the local surface morphology of the damage site to the PL image. A motorized XY stage (ANT130XY, Aerotech) is used to translate the sample to predefined coordinates for the shot sequence and PL imaging. A Renishaw Raman system with a 633 nm (1.96 eV) excitation laser was used to study the PL spectrum. Environmental SEM images (S-3400N, Hitachi) were taken for high resolution morphology analysis after the damage growth.

3. Results and discussions

Figure 1 provides an example of damage growth by showing a series of optical reflectance and PL images throughout the multi-shot process. Figure 1(a) shows an optical reflectance and wide-field PL image of a surface damage site with an effective circular diameter (ECD) of a few tens of micrometers. The initial site (Figs. 1(a) and (b)) shows a clear local PL intensity contrast with a stronger intensity at the periphery, implying a non-uniform distribution of defects that form

Optics EXPRESS

various energy levels within its bandgap [21]. After exposure to two more shots of the same fluence, the PL images (Fig. 1(d) and 1(f)) show changes in local intensity and shape which is attributed to absorption from laser induced defects [12,22]. A change in PL characteristics is not always accompanied by a visible change in the ECD as shown in Figs1a-g. However, when ECD growth is observed (Fig. 1(i)), it is often predicted with a large spike in PL intensity when compared with the prior shot (more than 10 times larger than the initial damage site) as shown in Fig. 1 h. This indicates a tendency for the defect structure to evolve significantly without a change in ECD. After an ECD change is detected, subsequent shots lead to rapid growth. We note that the number of shots and fluence required to observe changes in PL intensity contrast and shape is dependent on initial morphology and defect distribution and varies widely from site to site. More examples of damage site growth by multi-shot process can be found in the Supplement 1 (Fig. S2).

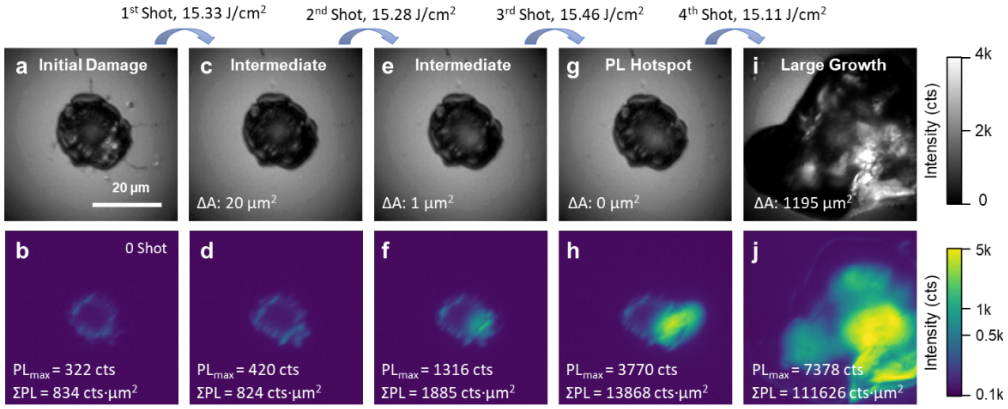

Fig. 1. Optical reflectance images (a, c, e, g, and i) and PL images (b, d, f, h, and j) showing a damage site that undergoes multiple nanosecond laser shots on input surface at laser fluences of 15.33 J/cm^2, 15.28 J/cm^2, 15.46 J/cm^2, 15.11 J/cm^2 for 1st, 2nd, 3rd, and 4th nanosecond laser shots, respectively. The series of images indicate initial damage (a-b), intermediate state (c-f), local PL intensity increase (g-h), and large growth (i-j). Panels after each shot, damage growth ($\Delta A = A_{post} - A_{pre}$), maximum PL ($PL_{max}$), and integrated PL hotspot with 80% threshold (ΣPL, defined in Eq. (1)) are depicted. The color bar for the PL images is in logarithmic scale. The scale bar indicates 20 µm.

We observe a strong relationship between the location of the observed PL change and damage propagation direction. Strong PL intensities usually appear at the periphery of a damage site where mechanical fractures and cracks are formed. Crack formation is attributed to the high stress field induced by rapid material heating and the associated thermal expansion. Figure 2 shows the optical reflectance image pre-shot and post-shot as well as the PL intensity overlaid onto the pre-shot optical reflectance image for four damage sites. After a subsequent shot, damage growth propagation near the location of the strong PL intensity can be observed indicated by the red arrows. The consistent observations in Figs. 1 and 2 imply that regions with the large PL intensities serve as light absorption centers which are prone to laser damage growth by a subsequent shot. Growth propagation is often accompanied in other directions (damage sites #1 and #3) indicated by the yellow dashed arrows. These areas potentially had damage prone structures such as cracks and fractures, which were mechanically ruptured by pressure wave propagation from light absorption centers.

Optical reflectance and PL images after each UV nanosecond laser shot from more than 100 damage sites are studied. Each site was shot until ECD growth was observed. To quantitatively

Optics EXPRESS

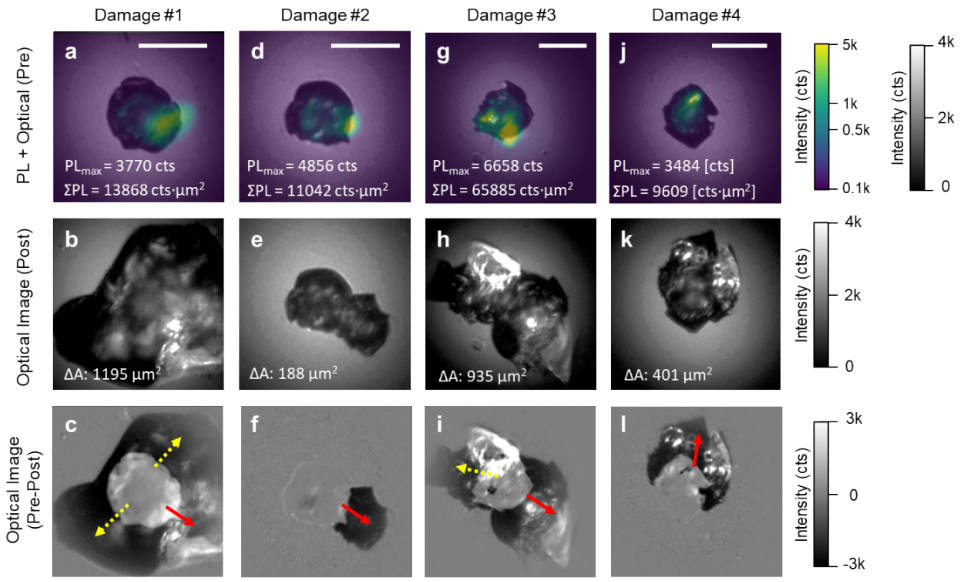

Fig. 2. Optical reflectance images showing correlation between local PL hotspot and laser damage growth. Optical images taken before (pre) nanosecond laser shot are overlaid with PL intensity images while the images taken after (post) laser shot and difference images of pre-shot and post-shot shot optical images show laser damage growth. The red arrows show the damage growth along the direction of the local PL hotspot while the dashed yellow arrows indicate the accompanied damage growth in other directions. Four damage sites were used: a-c) damage #1 (the same damage site shown in Fig. 1), d-f) damage #2, g-i) damage #3, and j-l) damage #4. For damage growth of each damage site, nanosecond laser shots with energy density of 15.11 J/cm^2, 13.60 J/cm^2, 14.20 J/cm^2, and 14.94 J/cm^2 were illuminated, respectively. Also, damage growth ($\Delta A = A_{post} - A_{pre}$), maximum PL ($PL_{max}$), and integrated PL hotspot with 80% threshold (ΣPL, defined in Eq. (1)) are depicted for each damage site. The color bar for the PL intensity images is in logarithmic scale. The scale bars indicate 20 μm. A full history of damage site growth is available in Supplement 1.

analyze the effect of local PL intensity on damage growth, we plot the integrated PL hotspot versus damage growth ($\Delta A = A_{post} - A_{pre}$, where A is the area) as shown in Fig. 3. We use the area change (ΔA) as an indicator of growth instead of ECD, as the local damage growth from the initial damage site often results in an irregular shape. By integrating the PL intensity, a site-specific and cumulative variable associated with PL is given (*i.e.*, integrated PL hotspot).

$$\sum PL = \iint I_{PL}(x,y)\, dxdy \quad (\text{if } I_{PL} > 0.8\, I_{PL,\,max}) \tag{1}$$

PL intensities within the damage site are integrated only if the local value is larger than 80% of the maximum PL intensity unless otherwise specified. This approach rejects random pixels that may not represent light absorption centers while also providing a quantitative effect of light absorption by the associated area. In many cases, no damage growth on the surface is observed even though the PL signature changes. This indicates that internal structural and/or defect states can form or evolve without an expansion of the exterior of the damage site similar to the cases shown in Figs. 1(a)-(h). However, if damage growth does occur, it tends to show a positive correlation with respect to the integrated PL hotspot (Figs. 3(a)). Figure 3(b) summarizes the plots shown in Fig. 3(a) by showing the probability of growth for sites greater than 200 μm^2 (*i.e.*, $\Delta A > 200$ μm^2) as a function of both laser fluence and integrated PL hotspot. It is observed

Optics EXPRESS

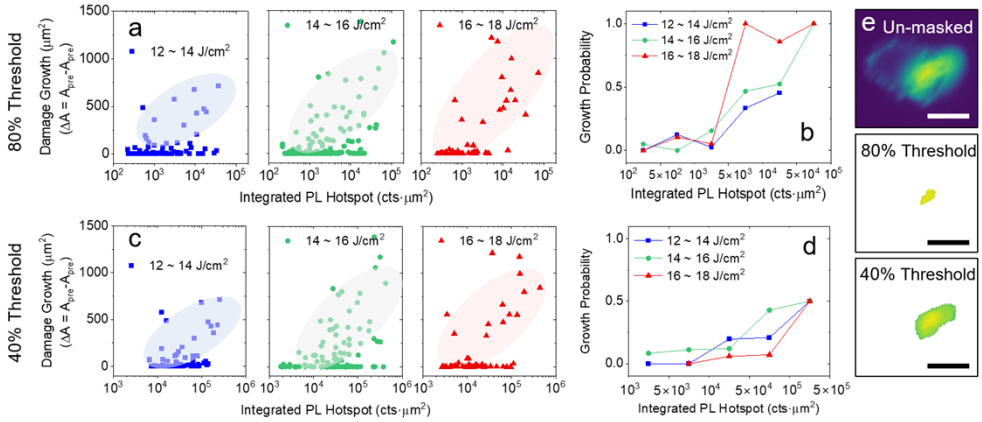

Fig. 3. Quantitative analysis based on integrated PL hotspot (Eq. (1)) against damage growth in area ($\Delta A = A_{post} - A_{pre}$) ($\mu m^2$). Panels a-b) and c-d) are subjected to a different PL thresholding, 80% and 40% of maximum PL intensity (*i.e.*, I_{PL}>0.8, I_{PL}>0.4, respectively). The plots depend on the various laser fluence ranges including 12~14 J/cm^2, 14~16 J/cm^2, and 16~18 J/cm^2. The ovals in panels a) and c) are the visual guide to show a positive correlation. b) and d) Probability of damage growth by more than 200 μm^2 depending on the integrated PL hotspot at various laser fluence ranges. e) An example of PL intensity images without thresholding (labeled as unmasked) and with 80% and 40% thresholding processes taken from Fig. 1 h. The scale bars are 10 μm.

that the correlation between growth probability and integrated PL hot spot becomes stronger as the laser fluence increases. Interestingly, when the integrated PL hotspot is obtained with a lower threshold value of 40%, (*i.e.*, $\sum PL$, if I_{PL}>0.4 $I_{PL,\,max}$), the positive relationship between the integrated PL hotspot and the laser fluence becomes less significant as shown in Fig. 3(d). The PL images processed by 80% of $I_{PL,\,max}$ occupy a smaller area with a higher PL intensity value compared to those processed with a 40% cutoff (Fig. 3(e), processed images from Fig. 1 h). A higher intensity threshold more accurately identifies local intensity hotspots related to light absorption centers, which is a more relevant indicator of damage growth than just integrating total PL intensity.

To understand the underlying mechanisms of large PL intensity and the resulting increase in damage growth probability, SEM images from the damage sites with an integrated PL hotspot larger than 10^3 cts·μm^2 were taken. This group of samples were prepared by illuminating sites with multiple shots until the integrated PL hotspot exceeds the threshold value. The maximum PL intensity generally occurs near cracks (Figs. 4(c), (f), and i), indicating that subsurface fractures contribute to the strong PL intensity. Meanwhile, from the other cracks indicated by yellow dashed boxes in Figs. 3(e) and (h), no significant PL intensity is observed, implying that the local defect density is a critical factor affecting the PL intensity. Previous studies revealed that the fractures generated under violent, high stress fields are more prone to laser damage [23]. The strong PL intensities observed in our experiment appear near the periphery of the damage site where mechanical fractures are dominant by ultrahigh stress field associated with pressure wave, while at the central crater, the melting and re-solidification process reduces such defects.

We measured PL spectra using a 633 nm (1.96 eV) excitation laser from the central low PL intensity crater (#3 in Fig. 5(a)), and the regions with strong PL intensity (#1 and #2 in Fig. 5(a)). We observed a sharp peak located at 650 nm (1.9 eV) from the central crater, which can be ascribed to the presence of non-bridging-oxygen hole centers (NBOHC) that are efficiently excited by photon energy near 2 eV [21]. Other types of defects such as oxygen deficient center

Optics EXPRESS

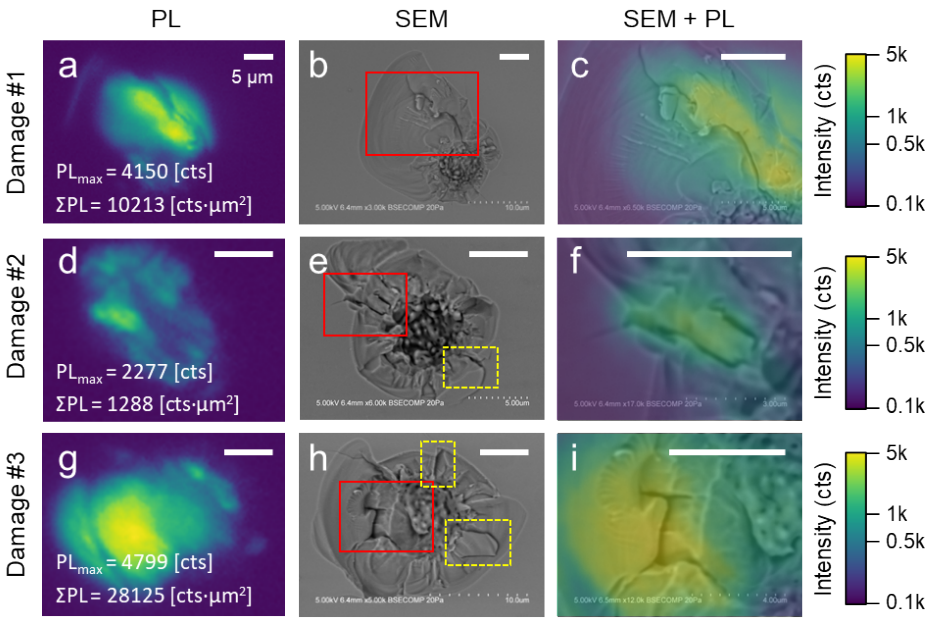

Fig. 4. PL and SEM images taken from damage sites #1 (a-c), #2 (d-f), and #3 (g-i). Images in the last column (c-i) show overlapped images of SEM and PL from the red boxes in the second column (b-h). The yellow dashed boxes in panels e-h show fractures without distinct local PL intensity. Maximum PL (PL_{max}), and integrated PL hotspot with 80% threshold (ΣPL, defined in Eq. (1)) are depicted. The color bars for the PL images are in logarithmic scale. All scale bars indicate 5 μm in the respective image.

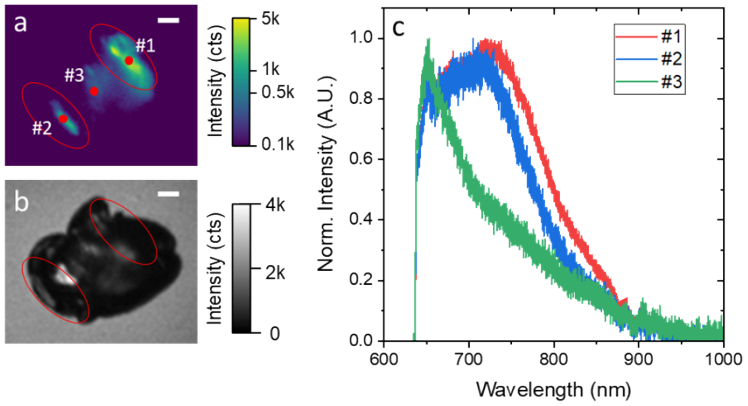

Fig. 5. a) PL and b) optical microscope images of a damage site with integrated PL hotspot of 2.78×10^4 counts, and c) normalized emission spectrum obtained from the spots #1, #2, and #3 indicated by the red dots in panel a). Note that the emission spectrum was obtained using 633 nm excitation laser. The color bar for the PL image is in logarithmic scale. The scale bars indicate 5 μm.

(ODC) and E′ cannot be detected, which requires a higher excitation photon energy. Meanwhile, from the regions with strong PL intensity, a broadened PL spectrum peaking at a lower energy (705 nm (1.76 eV)) appears, and the region with stronger PL intensity (#1 in Fig. 5(a)) shows a broader spectrum, spanning a longer range of wavelengths compared to the region with lower PL

Optics EXPRESS

intensity (#2 in Fig. 5(a)). The broad PL spectrum from silica damage sites has been ascribed to a high defect density that produces densely packed intermediate energy states in the silica electronic band structure [16,17]. Also, a cluster of silicon nanoparticles generated by a high temperature induced phase separation of silica has been identified as a potential source of the broad PL emission [24,25]. These possible origins of the broadened PL spectrum and the related high defect density can induce strong light absorption leading to larger laser damage growth. In addition, subsurface fractures and cracks with gaps close to the wavelength may enhance the electromagnetic field by interference effects [26], potentially contributing to the local PL intensity. Images taken with various polarization directions of the excitation laser beam show an identical shape and contrast, implying that interference effects have a negligible contribution toward the measured PL intensity.

4. Conclusion

In this study we showed how the strong local PL intensity induced by multi-shot process correlates with laser-induced damage growth. We observe an elevated local PL intensity after multi laser shots, which leads to significant growth from a subsequent laser shot. Our quantitative analysis shows that the laser damage growth probability clearly depends on the integrated PL hotspot of damage site. SEM imaging paired with a study of the PL spectrum shows that subsurface fractures and cracks with a high defect density act as light absorption centers responsible for a strong PL response and eventual laser damage growth. We believe that this study elucidates the underlying physical mechanisms of damage growth using rapid screening techniques, offering an effective strategy for mitigating optical damage. Future work involves developing spectrally resolved PL imaging, which can spatially identify different types of defects and their contributions to damage growth. The approach can further enhance the predictability of damage growth. Additionally, wide-field PL imaging for rapidly probing microscopic defects can be applied to examining local structural and optical defects in other dielectric optical materials as well as high bandgap semiconductors.

Funding. Lawrence Livermore National Laboratory (LLNL) Laboratory Directed Research and Development grant (22-ERD-003).

Acknowledgments. This work was performed under the auspices of the U.S. Department of Energy by Lawrence Livermore National Laboratory under Contract DE-AC52-07NA27344.

Disclosures. The authors declare no conflicts of interest.

Data availability. Data underlying the results presented in this paper are not publicly available at this time but may be obtained from the authors upon reasonable request.

Supplemental document. See Supplement 1 for supporting content.

References

1. N. D. Urban, K. R. P. Kafka, K. L. Marshall, *et al.*, "Laser-induced damage characteristics of fused silica surfaces polished to different depths using fluid jet polishing," Opt. Eng. **61**, 071604 (2022).
2. B. Bertussi, J.-Y. Natoli, and M. Commandre, "Effect of polishing process on silica surface laser-induced damage threshold at 355 nm," Opt. Commun. **242**, 227–231 (2004).
3. P. E. Miller, J. D. Bude, T. I. Suratwala, *et al.*, "Fracture-induced subbandgap absorption as a precursor to optical damage on fused silica surfaces," Opt. Lett. **35**, 2702–2704 (2010).
4. J. Fournier, J. Neauport, P. Grua, *et al.*, "Green luminescence in silica glass: A possible indicator of subsurface fracture," Appl. Phys. Lett. **100**, 114103 (2012).
5. Y. Zhong, Y. Dai, Y. Tian, *et al.*, "Effect on nanoscale damage precursors of fused silica with wet etching in KOH solutions," Opt. Mater. Express **11**, 884–894 (2021).
6. C. Cai, X. He, H. Zhao, *et al.*, "Effect of etching parameters on the surface quality and laser damage thresholds of fused silica with megasonic-assisted HF acid etching," in *9th International Symposium on Advanced Optical Manufacturing and Testing Technologies: Advanced Optical Manufacturing Technologies* (SPIE, 2019), Vol. 10838, pp. 428–435.
7. R. N. Raman, R. A. Negres, M. J. Matthews, *et al.*, "Effect of thermal anneal on growth behavior of laser-induced damage sites on the exit surface of fused silica," Opt. Mater. Express **3**, 765–776 (2013).

Optics EXPRESS

8. R. N. Raman, M. J. Matthews, J. J. Adams, *et al.*, "Monitoring annealing via CO_2 laser heating of defect populations on fused silica surfaces using photoluminescence microscopy," Opt. Express **18**, 15207–15215 (2010).
9. I. L. Bass, G. M. Guss, M. J. Nostrand, *et al.*, "An improved method of mitigating laser-induced surface damage growth in fused silica using a rastered pulsed CO2 laser," in *Laser-Induced Damage in Optical Materials: 2010* (SPIE, 2010), Vol. 7842, pp. 522–533.
10. R. A. Negres, G. M. Abdulla, D. A. Cross, *et al.*, "Probability of growth of small damage sites on the exit surface of fused silica optics," Opt. Express **20**, 13030–13039 (2012).
11. R. A. Negres, M. A. Norton, D. A. Cross, *et al.*, "Growth behavior of laser-induced damage on fused silica optics under UV, ns laser irradiation," Opt. Express **18**, 19966–19976 (2010).
12. S. G. Demos, M. Staggs, and M. R. Kozlowski, "Investigation of processes leading to damage growth in optical materials for large-aperture lasers," Appl. Opt. **41**, 3628–3633 (2002).
13. S. O. Kucheyev and S. G. Demos, "Optical defects produced in fused silica during laser-induced breakdown," Appl. Phys. Lett. **82**, 3230–3232 (2003).
14. S. G. Demos, M. Staggs, K. Minoshima, *et al.*, "Characterization of laser induced damage sites in optical components," Opt. Express **10**, 1444–1450 (2002).
15. T. A. Laurence, J. D. Bude, N. Shen, *et al.*, "Metallic-like photoluminescence and absorption in fused silica surface flaws," Appl. Phys. Lett. **94**, 151114 (2009).
16. T. A. Laurence, J. D. Bude, N. Shen, *et al.*, "Quasi-continuum photoluminescence: Unusual broad spectral and temporal characteristics found in defective surfaces of silica and other materials," J. Appl. Phys. **115**, 083501 (2014).
17. T. A. Laurence, S. Ly, J. D. Bude, *et al.*, "Energy transfer networks: Quasicontinuum photoluminescence linked to high densities of defects," Phys. Rev. Materials **1**, 065201 (2017).
18. Y. Rho, C. F. Miller, R. E. Yancey, *et al.*, "Wide-field probing of silica laser-induced damage precursors by photoluminescence photochemical quenching," Opt. Lett. **48**, 3789–3792 (2023).
19. M. C. Nostrand, T. L. Weiland, R. L. Luthi, *et al.*, "A large-aperture high-energy laser system for optics and optical component testing," in *Laser-Induced Damage in Optical Materials: 2003* (SPIE, 2004), Vol. 5273, pp. 325–333.
20. M. J. Runkel, A. K. Burnham, D. Milam, *et al.*, "Results of pulse-scaling experiments on rapid-growth DKDP triplers using the Optical Sciences Laser at 351 nm," in *Laser-Induced Damage in Optical Materials: 2000* (SPIE, 2001), Vol. 4347, pp. 359–372.
21. L. Skuja, H. Hosono, and M. Hirano, "Laser-induced color centers in silica," in *Laser-Induced Damage in Optical Materials: 2000* (SPIE, 2001), Vol. 4347, pp. 155–168.
22. S. G. Demos, R. N. Raman, and R. A. Negres, "Time-resolved imaging of processes associated with exit-surface damage growth in fused silica following exposure to nanosecond laser pulses," Opt. Express **21**, 4875–4888 (2013).
23. N. Shen, P. E. Miller, J. D. Bude, *et al.*, "Thermal annealing of laser damage precursors on fused silica surfaces," Opt. Eng **51**, 121817 (2012).
24. S. Xu, X. Yuan, X. Zu, *et al.*, "Laser-induced defects in fused silica by UV laser irradiation," J. Non-Cryst. Solids **353**, 4212–4217 (2007).
25. K. Sato, N. Kishimoto, and K. Hirakuri, "White luminescence from silica glass containing red/green/blue luminescent nanocrystalline silicon particles," J. Appl. Phys. **102**, 104305 (2007).
26. M. Chambonneau and L. Lamaignère, "Multi-wavelength growth of nanosecond laser-induced surface damage on fused silica gratings," Sci. Rep. **8**, 891 (2018).